

RESTORATION OF THE BEARING CAPACITY OF DAMAGED TRANSPORT CONSTRUCTIONS MADE OF CORRUGATED METAL STRUCTURES

VITALII KOVALCHUK¹, MYKOLA SYSYN^{2*},
YURIY HNATIV³, ARTUR ONYSHCHENKO¹,
MAKSYM KOVAL⁴, OLEKSII TIUTKIN³, MARIANA PARNETA⁴

¹*National Transport University, Kyiv, Ukraine*

²*Institute of Railway Systems and Public Transport,
Technical University of Dresden, Dresden, Germany*

³*Dnipro National University of Railway Transport, Dnipro, Ukraine*

⁴*Institute of Architecture and Design,
Lviv Polytechnic National University, Lviv, Ukraine*

Received 6 April 2020; accepted 9 October 2020

Abstract. The paper deals with damages of transport constructions made of corrugated metal structures in the body of a railway track or a road during their operation. A constructive variant to restore the bearing capacity of structures was developed, which consists of installing an annular stiffening rib into the concave part of the corrugated metal profile. The main advantage of this method compared to the double corrugating method is the possibility of performing the reinforcement works during structure operation without interrupting the

* Corresponding author. E-mail: mykola.sysyn@tu-dresden.de

Vitalii KOVALCHUK (ORCID ID 0000-0003-4350-1756)

Mykola SYSYN (ORCID ID 0000-0001-6893-0018)

Yuriy HNATIV (ORCID ID 0000-0001-8862-4202)

Maksym KOVAL (ORCID ID 0000-0003-1244-1738)

Oleksii TIUTKIN (ORCID ID 0000-0003-4921-4758)

Mariana PARNETA (ORCID ID 0000-0001-9459-3676)

Copyright © 2021 The Author(s). Published by RTU Press

This is an Open Access article distributed under the terms of the Creative Commons Attribution License (<http://creativecommons.org/licenses/by/4.0/>), which permits unrestricted use, distribution, and reproduction in any medium, provided the original author and source are credited.

movement of transport vesicles. The study has proved that the reinforcement method significantly increases the carrying capacity of corrugated metal structures. A numerical finite element model was developed to determine the stress-strain state of structures made of corrugated metal structures reinforced with round stiffening ribs. The soil pressure on the corrugated shell in the model is taken into account with the application of radial and axial forces on the outer surface of the shell. It was determined that the most appropriate location of the ribs is in the centre of the building, where the reinforcement area corresponds to the width of the road or railway line. The advantage of this approach is the ability to more efficiently distribute the reinforcement material by selecting the ribs in the most loaded sections of corrugated metal structures.

Keywords: corrugated metal structures, deformation, railway track, stress.

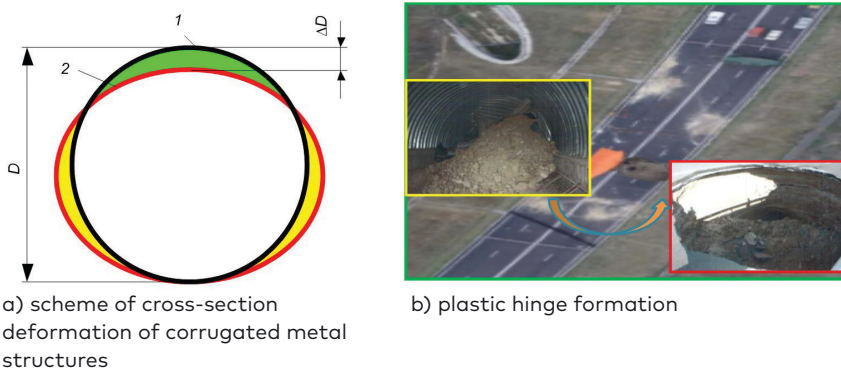
Introduction

Corrugated metal structures (CMSs) have several advantages over reinforced concrete structures. Implementation of structures made of CMS in transport construction promises both economically and because of the shortened building period. However, under conditions of operational loads and the increase of CMS cross-sections, they have insufficient bearing capacity. It is caused by the appearance of residual deformations in the vertical and horizontal directions (Figure 1a), loss of stability of the structure shape and even the formation of plastic hinges (Gerber et al., 2016; Kovalchuk et al., 2016, 2017a, 2017b, 2018). The unfavourable conditions of operational loadings are caused by the vehicle weight and dynamic vibration while passing road irregularities. The irregularities like transition zones and rail joints cause high dynamic vibration (He et al., 2021), which accelerates the residual deformation of the CMS that has sensitive to vibration soil filling. An additional factor influencing the CMS carrying capacity is temperature loading (Chen et al., 2020). The factors can have serious consequences in case of their unfavourable combination. For example, on the location km 1+350 road of Simferopol–Yevpatoria–Myrne–Dubky highway, the roadbed over the transport construction with CMS was destroyed, caused by the formation of a plastic hinge in the metal of the structure (Figure 1b).

The loss of the cross-sectional shape of the construction adversely affects both functional properties of a railway or a highway and its construction. It causes the formation of the pits on a roadway or unevenness appearance on a railway track over CMS and the appearance of residual deformations and stresses. In the United States, Ohio, more than 900 CMSs built-in 1951–1965 were surveyed. As a result, it was found that the loss of bearing capacity of structures with CMS occurred

during cross-section deformations from 22% to 34% in the vertical direction, and complete constructions collapse during cross-section deformations from 45% to 55% in the same direction. The studies have demonstrated that in 95% of cases, the destruction of constructions with CMS occurred due to poor soil compaction. Therefore, it was decided to limit the amount of structures deformation of annular shape to 2% of the vertical or horizontal diameters, and for box structures – to 0.5% (Esmaeili et al., 2013; Mak et al., 2009), which allows obtaining the safety coefficient of construction operation within 2–5. The study (Mak et al., 2009) indicates that CMS are flexible structures that are very “sensitive” to any deviations from the technological process at the construction, which may cause premature failures during the following operation.

The quality of the design works is of great importance for ensuring durability and safe operation of transport facilities with CMS. At the stage of such constructions design, it is necessary to consider the deterioration of materials performance over time due to environmental aggression. In addition, the axial load increase due to the settlements caused by vehicles movement during construction operation. Therefore, structural options for restoring the load-bearing capacity of constructions with CMS at minimal economic cost is an urgent problem. Another cost-effective approach, which is frequently presented in studies over the last years (Abdelkader et al., 2020), is based on applying autonomous monitoring means together with the artificial intelligence methods. The methods allow to predict the bridge defects and avoid



Note: D – design diameter of the construction cross-section; ΔD – the amount of deformation; 1 – design position; 2 – deformed state.

Figure 1. The roadbed destruction due to the plastic hinge defect in the corrugated metal structure

unexpected damages. Thus, the purpose of the work is to develop the method of load-bearing capacity restoration of damaged transport constructions made of CMSs and the survey of the stress-strain state of these constructions.

1. Method for increasing the bearing capacity of corrugated metal structures

The method of double-corrugation is used today to restore the load-bearing capacity of damaged transport constructions made of CMS with a large cross-sectional area (Korusiewicz & Kunecki, 2011; Nabochenko et al., 2019).

The double corrugation is be used for all cross-sectional shapes of CMSs (Flener, 2009; Gerber et al., 2019; Machelski, 2013; Maleska & Beben, 2019; Pettersson et al., 2015). Such stiffeners are most widely used for box structures with large cross-sections in which the bending stiffness in the vault of the structure is problematic to provide. The problems of contact interaction of two corrugated metal shells during the CMS transport constructions reinforcement are considered in the studies (Karpiuk et al., 2019a; Machelski, 2013, 2015; Pettersson et al., 2017). It is noted that the stiffeners are installed in the most loaded areas of the structure for cost reduction. The experimental tests of the box-corrugated structures reinforced with transverse stiffeners have shown that the load resistance of structures at the vault level is increased more than twice compared to the non-reinforced structures (Pettersson et al., 2017).

The studies (Ahaieva et al., 2019; Karpiuk et al., 2019a, 2019b) propose a possible reinforcement of the longitudinal reinforced concrete stiffeners, symmetrically on both sides of the CMS. The technological schemes of the CMS reinforcement using the external transverse stiffeners of the BridgeCor External Rib System are presented in (Contech Engineered Solutions, 2019). This system of external ribs BridgeCor optimises the material of the structure, which saves costs, reduces the amount of material required, allows to increase the size of the span of the structure and its stability. Numerical, analytical and experimental studies (Maleska & Beben, 2019) has found out that the deformation of the structure by using the double corrugation and filling the internal space with concrete is 54% less than for the structure without transverse stiffeners. The deformation is 34% lower than that with the additional corrugation. Liu et al. (2020) present an application of dynamic distributed fibre optic strain sensors that

were used to monitor the behaviour of an in-service corrugated steel culvert with a span of 2.75 m and a skew angle of 45° under static and dynamic vehicle loading. Maximum thrust envelopes were developed using the distributed data and demonstrated that positions near the crown experienced thrusts higher than those at the spring lines. The peak measured strain was 9.3% of the yield strain, suggesting that the culvert had adequate live load capacity. The authors in the study (Beben, 2017) carried out the numerical calculations under static live loads for the corrugated steel plate culvert with a span of 12.315 m and a height of a shell of 3.555 m. The study also shows the numerical calculations for the actual culvert, which previously had been studied experimentally. The author validated the obtained numerical results to the results of experiments. Parametric analysis showed that the angle of internal friction was a major factor in corrugated steel plate culverts. The paper (Beben, 2009) presents a numerical analysis of the soil-steel bridge, which was also thoroughly tested under real field loads (during backfilling and under static loads). The research (Beben, 2013) demonstrates the results and conclusions from field tests under service loads conducted on a corrugated steel plate road culvert. Based on the measured displacements, using the fast Fourier transform method, the dominant frequencies of the culvert were determined. This study (Beben, 2014) presents the results and conclusions of field tests under service loads conducted on a corrugated steel plate railway culvert. Inductive gauges, extensometers, and accelerometers were used to monitor displacements, strains, and accelerations of this culvert, respectively. The biggest displacements and strains were recorded at the culvert crown and quarter points, respectively. The results of a numerical analysis performed on a corrugated steel plate bridge during a backfilling process are presented by Beben (2012). The analysed bridge structure was a box culvert having a span of 12.315 m and a clear height of 3.550 m). Obtained calculation results were compared to the experimental ones. The application of the Fast Lagrangian Analysis of Continua (FLAC) program based on the finite differences method (FDM) to determine the behaviour of the soil-steel bridge structure during backfilling is presented. The assumptions of a computational 2D model of the soil-steel structure with a nonlinear interface layer are described. The objective of this study (Orton et al., 2015) was to determine the effects of live load (truckloads) on reinforced concrete box culverts classified as bridges (spans longer than 6 m [20 ft]) under soil fills of different thicknesses. The study considered the field testing of 10 existing reinforced concrete box culverts with fill depths ranging from 0.76 m to 4.10 m. In the article (Sanaeiha et al., 2017), a field test of a large-span soil-steel bridge is described. The case study involved

a corrugated steel plate that was stiffened by concrete rings. The rings were applied to make it possible to use only one layer of the steel plate while covering 20 m. The test involved deflection and strain measurements of the steel plate under increasing layers of soil. The test results show that maximum deflection and the maximum bending moment occurred at the crown when the soil reached the crown level. Conversely, the maximum axial force occurred at the bottom of the arch when the soil reached its maximum level above the arch. The test results were compared to the well-known design methods of soil steel bridges. Conforming to the results, the design methods are conservative in predicting bending moments, but they are more realistic in predicting axial forces. This study (Sheldon et al., 2015) investigates the field performance of culvert joints in five existing pipe culverts. Test culverts consisted of two corrugated metal culverts, two reinforced concrete culverts, and one high-density polyethene culvert. The results indicate that separation at the joint was quite significant at times. In the worst case, the measured separation at the joint was equal to 50% of the measured deflection. Strains measured near the joint in steel culverts were significantly smaller than the yield strain. The dynamic deflections were typically 10%–40% less than the static deflections.

It is noted that such reinforcement can be performed only during the building of the construction with CMS. However, in 90% of cases of constructions with CMS, the damage occurs under service conditions. Therefore, improved design options are developed to restore the load-bearing capacity of these facilities during operation. For this purpose, the method of additional stiffeners installation – metal rods with a diameter of 16 mm built into the waves of the corrugated structure profile (Figure 2) – is proposed. The other diameters require the estimation of CMS for the particular loading.

Strengthening the structure with metal stiffening ribs is suggested at the places of action of the greatest bending moments caused by

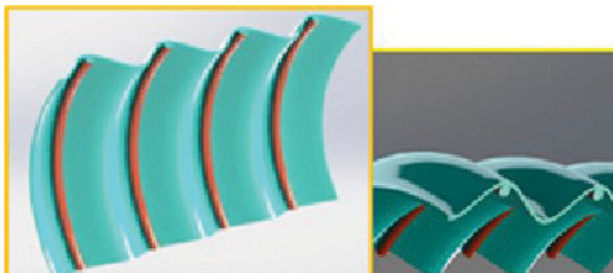


Figure 2. Corrugated metal structure with additional transverse stiffeners

transport movement. It is most advisable to install stiffeners in the central part of the structure so that the reinforcement zone occupies the width of a carriageway or a railway track (Figure 3).

The stiffeners are attached to the CMS by welding. The problem of the protective coating at the installation place of the stiffeners is solved by applying an anti-corrosion coating. The width of the reinforcement part under the road or railway is 2400 mm, which is sufficient for the rail track gauge 1520 mm with the wave of corrugation 150×50 mm. The number of stiffening ribs for the other parameters of the corrugation wave is determined, taking into account the principle that the strengthening width should involve the overall carriageway and a half of it on both sides.

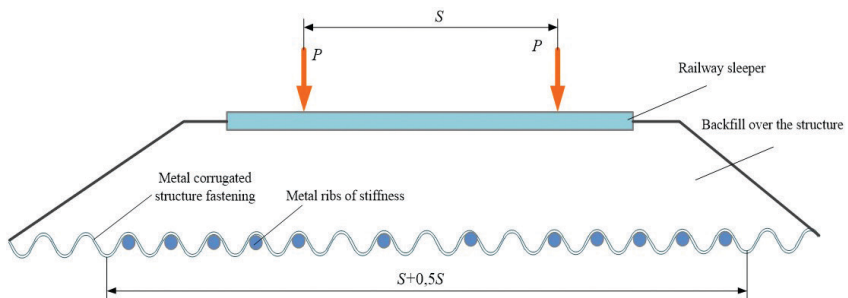
The advantage of this approach is distributing the material more rationally by installing stiffeners in the most loaded cross-sections of the CMS. However, the proposed design solution changes the design scheme of the structure and requires the methodology developed for the study of the stress-strain state of reinforced structures.

2. Mathematical model

The elastic corrugated cylindrical coating assigned to the cylindrical coordinate system r, φ, z ($0 \leq \varphi < 2\pi$) is presented in Figure 4. The inner S_1 and outer S_2 surfaces of the coating are described by the Eqs (1–4) respectively.

$$r = r_1 + \varepsilon \sin \alpha z; \quad (1)$$

$$r = r_2 + \varepsilon \sin \alpha z, \quad (2)$$



Note: S – width among wheel pairs of moving vehicles; P – loads from moving vehicles.

Figure 3. Scheme of transport structure reinforcement with transverse stiffening ribs

where r_1, r_2 – radii of cylindrical base surfaces, and $r_1 < r_2$; ε – wave amplitude; α – corrugation frequency. The thickness of the shell is $t = r_1 - r_2$.

Coating along the line

$$\left\{ \begin{array}{l} r = r_1 + \varepsilon, \\ z = \frac{\pi}{\alpha} \left(\frac{1}{2} + 2n \right), \quad n = 0, \pm 1, \pm 2, \dots, \end{array} \right. \quad (3)$$

reinforced with annular ribs of stiffness, which occupied areas.

$$(V_n) = \left\{ (r, \varphi, z) : r_0 - \sqrt{R^2 - (z - z_{0n})^2} \leq r \leq r_0 + \sqrt{R^2 - (z - z_{0n})^2}, \right. \\ \left. 0 \leq \varphi < 2\pi, z_{0n} - R \leq z \leq z_{0n} + R \right\}, \quad (4)$$

where $r_0 = r_1 + \varepsilon - R$; $z_{0n} = \frac{\pi}{\alpha} \left(\frac{1}{2} + 2n \right)$; R – radius of a circle, which is a cross-section of a stiffening rib.

Considered covering is under the action of forces $P_r(\varphi, z)$, $P_z(\varphi, z)$ applied to the outer surface S_2 . The inner surface S_1 and the stiffening ribs except for lines Eq. (3) are load free. The lateral surfaces $z = \pm l$ of the coating are also load-free.

Suppose that conditions of perfect mechanical contact of the coating with stiffening ribs are performed on the lines Eq. (3).

To determine the stress-strain state of the coating and stiffening ribs, the Eqs (5–8) and relations of the theory of elasticity are used. The equilibrium equations of the elementary volume of the bodies under consideration are as follows:

$$\frac{\partial \sigma_{rr}}{\partial r} + \frac{1}{r} \frac{\partial \sigma_{r\varphi}}{\partial \varphi} + \frac{\partial \sigma_{rz}}{\partial z} + \frac{\sigma_{rr} - \sigma_{\varphi\varphi}}{r} = 0,$$

$$\frac{\partial \sigma_{r\varphi}}{\partial r} + \frac{1}{r} \frac{\partial \sigma_{\varphi\varphi}}{\partial \varphi} + \frac{\partial \sigma_{\varphi z}}{\partial z} + \frac{2\sigma_{r\varphi}}{r} = 0,$$

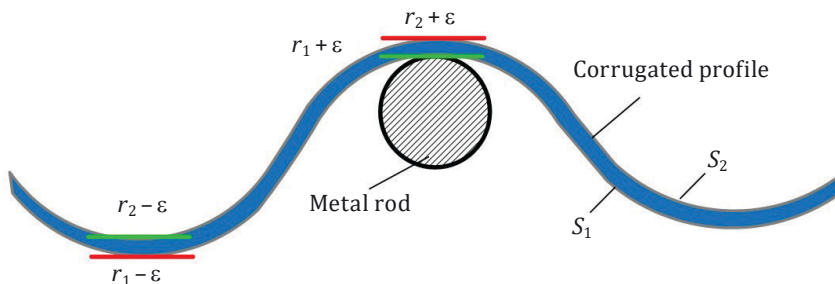


Figure 4. Scheme to the description of the mathematical model of the task

$$\frac{\partial \sigma_{rz}}{\partial r} + \frac{1}{r} \frac{\partial \sigma_{\varphi z}}{\partial \varphi} + \frac{\partial \sigma_{zz}}{\partial z} + \frac{\sigma_{rz}}{r} = 0, \quad (5)$$

where σ_{ij} ($i, j = r, \varphi, z$) – components of the stress tensor.

Components of deformation tensor ε_{ij} ($i, j = r, \varphi, z$) and displacement vector u_i ($i = r, \varphi, z$) relate to correlations Eq. (6):

$$\begin{aligned} \varepsilon_{rr} &= \frac{\partial u_r}{\partial r}, \varepsilon_{\varphi\varphi} = \frac{1}{r} \left(u_r + \frac{\partial u_\varphi}{\partial \varphi} \right), \varepsilon_{zz} = \frac{\partial u_z}{\partial z}, \\ \varepsilon_{r\varphi} &= \frac{1}{2} \left(\frac{1}{r} \frac{\partial u_r}{\partial \varphi} + \frac{\partial u_\varphi}{\partial r} - \frac{u_\varphi}{r} \right), \\ \varepsilon_{\varphi z} &= \frac{1}{2} \left(\frac{\partial u_\varphi}{\partial z} + \frac{1}{r} \frac{\partial u_z}{\partial \varphi} \right), \varepsilon_{rz} = \frac{1}{2} \left(\frac{\partial u_r}{\partial z} + \frac{\partial u_z}{\partial r} \right). \end{aligned} \quad (6)$$

Stress σ_{ij} and deformation ε_{ij} relate to correlations of Hooke Law, which take the form:

$$\begin{aligned} \sigma_{rr} &= 2G \left(\varepsilon_{rr} + \frac{\nu\theta}{1-2\nu} \right), \\ \sigma_{\varphi\varphi} &= 2G \left(\varepsilon_{\varphi\varphi} + \frac{\nu\theta}{1-2\nu} \right), \\ \sigma_{zz} &= 2G \left(\varepsilon_{zz} + \frac{\nu\theta}{1-2\nu} \right), \\ \sigma_{r\varphi} &= 2G\varepsilon_{r\varphi}, \sigma_{\varphi z} = 2G\varepsilon_{\varphi z}, \sigma_{rz} = 2G\varepsilon_{rz}, \end{aligned} \quad (7)$$

where $\theta = \varepsilon_{rr} + \varepsilon_{\varphi\varphi} + \varepsilon_{zz}$; G – displacement modulus; ν – Poisson coefficient.

The periodicity conditions of the stress-strain state of the coating and the stiffening ribs relative to coordinate φ is be presented in the form:

$$\begin{aligned} \sigma_{r\varphi} \Big|_{\varphi=0} &= \sigma_{r\varphi} \Big|_{\varphi=2\pi-0}, \\ \sigma_{\varphi\varphi} \Big|_{\varphi=0} &= \sigma_{\varphi\varphi} \Big|_{\varphi=2\pi-0}, \\ \sigma_{\varphi z} \Big|_{\varphi=0} &= \sigma_{\varphi z} \Big|_{\varphi=2\pi-0}, \\ u_r \Big|_{\varphi=0} &= u_r \Big|_{\varphi=2\pi-0}, \\ u_\varphi \Big|_{\varphi=0} &= u_\varphi \Big|_{\varphi=2\pi-0}, \\ u_z \Big|_{\varphi=0} &= u_z \Big|_{\varphi=2\pi-0}. \end{aligned} \quad (8)$$

Conditions of the ideal mechanical contact of considered bodies take the form Eq. (9):

$$\begin{aligned}
 \sigma_{rr}(r_1 + \varepsilon - 0, \varphi, z_{0n}) &= \sigma_{rr}(r_1 + \varepsilon + 0, \varphi, z_{0n}), \\
 \sigma_{r\varphi}(r_1 + \varepsilon - 0, \varphi, z_{0n}) &= \sigma_{r\varphi}(r_1 + \varepsilon + 0, \varphi, z_{0n}), \\
 \sigma_{rz}(r_1 + \varepsilon - 0, \varphi, z_{0n}) &= \sigma_{rz}(r_1 + \varepsilon + 0, \varphi, z_{0n}), \\
 u_r(r_1 + \varepsilon - 0, \varphi, z_{0n}) &= u_r(r_1 + \varepsilon + 0, \varphi, z_{0n}), \\
 u_\varphi(r_1 + \varepsilon - 0, \varphi, z_{0n}) &= u_\varphi(r_1 + \varepsilon + 0, \varphi, z_{0n}), \\
 u_z(r_1 + \varepsilon - 0, \varphi, z_{0n}) &= u_z(r_1 + \varepsilon + 0, \varphi, z_{0n}).
 \end{aligned} \tag{9}$$

Let S be the union of the surface S_1 and the surfaces of the stiffening ribs from which the lines Eq. (3) are taken. In this case, the conditions at the boundary of the coating and the stiffening ribs take the form:

$$\begin{aligned}
 (\sigma_{rr}n_r + \sigma_{rz}n_z)|_S &= 0, (\sigma_{r\varphi}n_r + \sigma_{\varphi z}n_z)|_S = 0, (\sigma_{rz}n_r + \sigma_{zz}n_z)|_S = 0, \\
 (\sigma_{rr}n_r + \sigma_{rz}n_z)|_{S_2} &= P_{(\varphi,z)r}(\sigma_{r\varphi}n_r + \sigma_{\varphi z}n_z)|_{S_2} = 0, \\
 (\sigma_{rz}n_r + \sigma_{zz}n_z)|_{S_2} &= P_z(\varphi, z), \\
 \sigma_{rz}|_{z=\pm l} &= 0, \sigma_{\varphi z}|_{z=\pm l} = 0, \sigma_{zz}|_{z=\pm l} = 0,
 \end{aligned} \tag{10}$$

where n_r, n_z – directing cosines of vectors of a single external normal to the surfaces of the considered bodies.

The surfaces S_1 correspond to the values

$$n_r = -\frac{1}{\Delta}, n_z = \frac{\varepsilon\alpha \cos\alpha z}{\Delta}, \tag{11}$$

and surfaces S_2 values

$$n_r = \frac{1}{\Delta}, n_z = -\frac{\varepsilon\alpha \cos\alpha z}{\Delta}. \tag{12}$$

In expressions (11) and (12), the value Δ is determined by the Eq. (13):

$$\Delta = \sqrt{1 + (\varepsilon\alpha \cos\alpha z)^2}. \tag{13}$$

Those parts of the surfaces of the stiffening ribs described by the Eqs (14) and (15)

$$r = r_0 + \sqrt{R^2 - (z - z_{0n})^2}, \quad (14)$$

correspond to directing cosines

$$n_r = \frac{\sqrt{R^2 - (z - z_{0n})^2}}{R}, n_z = \frac{z - z_{0n}}{R} \quad (15)$$

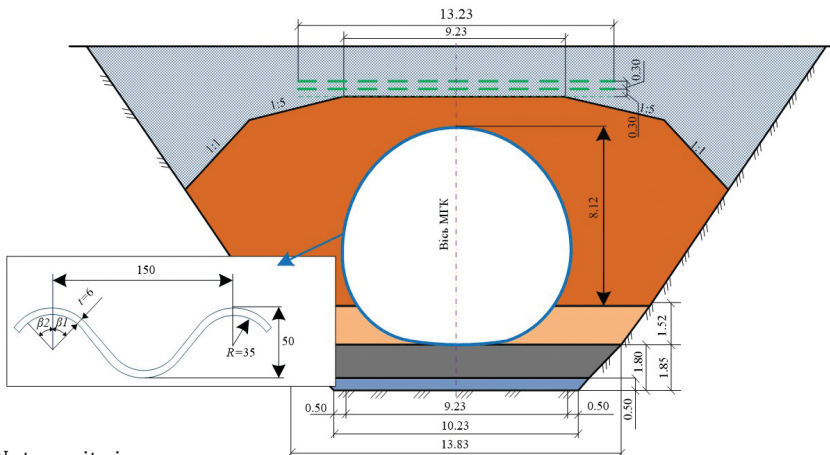
and the parts of surfaces of stiffening ribs described by the Eq. (16)

$$r = r_0 + \sqrt{R^2 - (z - z_{0n})^2} \quad (16)$$

correspond to directing cosines (Eq. (17))

$$n_r = -\frac{\sqrt{R^2 - (z - z_{0n})^2}}{R}, n_z = \frac{z - z_{0n}}{R}. \quad (17)$$

Then, in agreement with the above method, the stress-strain state of the construction with CMS reinforced with stiffening ribs is investigated.



Note: units in m.

Figure 5. Cross-section of the construction with corrugated metal structures

3. Stress-deformed state modelling and analysis

Consider the construction designed for road and railway transport passage. The horizontal diameter of the construction is 9.23 m, and the vertical diameter is 8.12 m (Figure 5).

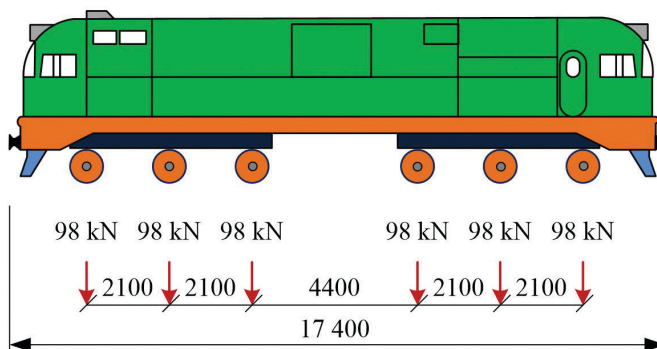
The soil backfill above the CMS at a length of 13.23 m is reinforced with metal stiffeners arranged in three rows vertically.

The construction metal sheets are made of corrugated structures of Multiplate MP 150 type, the corrugation wavelength of 150 mm, the height is 50 mm, and the thickness is 6 mm. The modulus of elasticity of the CMS and the stiffening ribs are taken to be equal to $E = 2.10 \cdot 10^5$ MPa, and the Poisson coefficients of CMS and stiffening ribs are $\nu = 0.25$.

The soil backfill has the following physical parameters: bulk density $\rho = 1.90$ t/m³, specific density $\rho_s = 2.65$ t/m³, the bulk weight of the backfill soil $\gamma_{cv} = 19.00$ kN/m³, internal friction angle $\varphi_{cv,k} = 41.90^\circ$. It is accepted that the degree of compaction of the soil backfill is 0.98, and its modulus of elasticity $E_s = 24.00$ MPa. The backfill height above the arch of the CMS is 2.00 m.

The static load on the structure was set from the locomotive series 2M62 with the following operating parameters: static weight 116 t, load from one axle of wheel pair 98 kN, the distance between among axles of wheel pairs 2100 mm, the distance among carts 8600 mm and total length of locomotive 17.55 m (Figure 6).

The loading of the rolling stock is expressed in so-called equivalent loads that consider the static and dynamic properties of rolling stock, train velocities, the superstructure and the subgrade properties. Nevertheless, the train and track dynamic interaction and, therefore, the sleeper loadings are subjected to many factors like the variable stiffness



Note: units in mm.

Figure 6. Scheme of a three-axle locomotive of the series 2M62

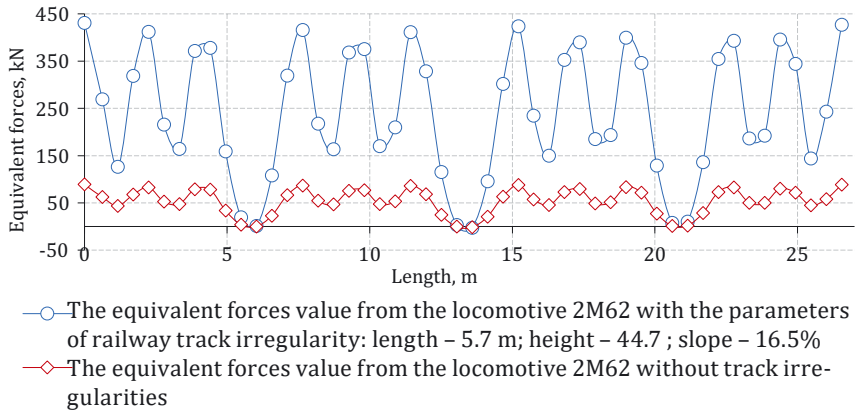


Figure 7. Equivalent forces while 2M62 locomotive passage along the track under sub-base elastic modulus 92.10 MPa

of the subgrade in the CMS zone or the sleeper-ballast interaction. Considering the factors like in the studies (Kurhan et al., 2016, 2020; Orosz et al., 2020; Shvets et al., 2020) could potentially decrease the uncertainty of the estimation of the equivalent loads. The distribution of equivalent loads (Figure 7) on sleepers along the track was obtained based on the track calculations for strength in consonance to the value of a sub-base elasticity modulus equal to 92.10 MPa.

Figure 6 shows that on the length of the railway track $S = 25.00$ m, the maximum equivalent force is 423.60 kN for the possible irregularities formed during the operation of the transport structure like Multiplate MP 150.

Further, calculating the stress-strain state of structures reinforced with transverse stiffening ribs is performed.

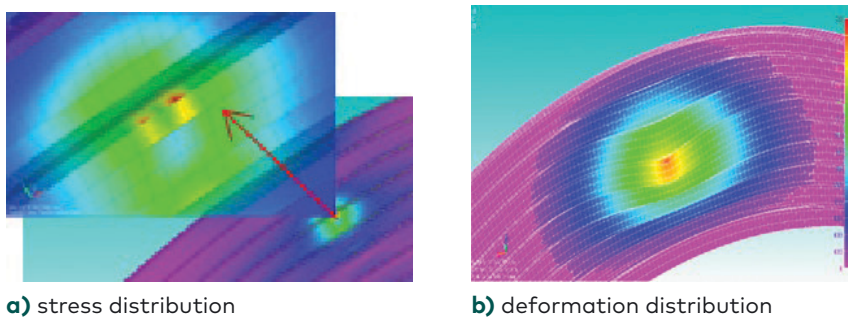


Figure 8. Stress-deformed state of a transport construction made of corrugated metal structure reinforced with stiffening ribs

4. Assessment of the stress-strain state of a corrugated metal structure reinforced with stiffeners

Consider the option of CMS reinforcement with a 16 mm diameter rod built into the waves of this corrugated structure. The wall thickness of the structure is 6 mm. The finite element model consists of 453 917 nodes and 146 586 finite elements. The results of stress and strain distribution in the CMS are shown in Figure 8.

Parabolic elements with intermediate nodes on the sides were used in the finite element modelling of the reinforced CMS. On the one hand, such elements better model the geometry of curved surfaces of parts. On the other hand, it reduces the number of finite elements and simultaneously increases the approximation of the functions of deformations stresses.

The metal pipe is modelled with flat finite elements 2D of the Plate type, and the space of the soil in the corrugated sinuses is filled with tetrahedra, and then with the distance from the shell, the soil is modelled with hexahedra. The concentration of the finite element grid was performed in the places of possible stress concentration and in the areas of contact of contacting bodies “soil backfill-metal structure“. Near the corrugations, the dimensions of the finite elements were chosen smaller, and the rest of the area was divided into elements of larger dimensions.

The boundary conditions at the surface “soil-metal shell“ correspond to the complete coincidence of nodal points of finite conjugate elements. The mentioned consideration is based on the assumption that corrugation increases the adhesion of the metal with soil.

The simulation of nonlinear structures using a perfectly plastic model, namely for plastic deformation in the corrugated metal construction in the settlements, uses von Mises criterion. In this case, to the parameters of elasticity: modulus of elasticity and Poisson ratio and density are completed with the yield strength of the CMS metal structure.

Six constants were set for ideal-plastic soil models such as Moore-Coulomb and Drucker-Prager: two elastic characteristics – the deformation modulus and the Poisson ratio; density; three characteristics of plasticity – the internal angle friction, the coefficient of adhesion and the angle of dilation.

In the nodes of the lower part of the soil, fixed hinges are used, making it impossible to move the structure in the vertical and horizontal directions linearly. In the nodes of the elements of the side faces, a fixation of horizontal movements is introduced.

The stresses in the CMS of 6 mm thickness, reinforced with additional stiffeners, are three times less than in the corresponding non-reinforced structure. The maximum stresses in the CMS wall are 23.55 MPa, and the maximum deformations are 2.92 mm.

A comprehensive indicator of the effectiveness of the design solution is used that takes into account the technical characteristics of the reinforced structure and its economic components to evaluate the effectiveness of the proposed structural solution. Eq. (18) determines it:

$$e = \sigma_e + E_e, \quad (18)$$

where σ_e is a technical indicator of the effectiveness of the design solution, %; E_e is a coefficient, which considers the cost of the basic technical solution and the volume of construction works to increase and their cost, %.

Eq. (18) determines the technical indicator of the effectiveness of the design solution:

$$\sigma_e = \frac{[\sigma]}{\sigma_{\max}}, \quad (19)$$

where $[\sigma]$ is the elastic limit of the CMS; σ_{\max} is the maximum stress obtained by the proposed design solution.

The integrated approach allows considering several factors, which influence the effectiveness of the proposed technical solution. These factors include the change in the cost of construction materials, the increase of construction costs due to additional materials, the increased complexity due to the additional volume of construction works.

The coefficient E_e is determined by the Eq. (20):

$$E_e = \frac{C}{C+c}, \quad (20)$$

where C is the cost of CMS of the basic technical solution, Euro; c is the cost of additional materials for structural reinforcement, thousand Euro.

Determination of the coefficient of increase in the cost of E_e construction is made based on data on the average cost of structures and materials of domestic manufacturers of CMS. These values are given in Table. It is assumed that the cost of a corrugated sheet of 1 mm thickness, which corresponds to the basic technical solution, is 235.00 Euro/t.

With a given level of loads on the transport construction, the stress in a noncorrugated metal structure with a thickness of 6 mm and a CMS with a thickness of 2 mm equals 361.60 MPa. It exceeds the permissible limit of elasticity of a metal, which is equal to 235.00 MPa. In other

design variants, the normal stresses of CMS in the cross-sections is lower than the steel yield strength; thus, each of these variants effectively increases the bearing capacity of CMS and prevents the transformation of a CMS into the plastic state.

With the reinforcement of CMS with additional stiffening ribs – annular rods – the efficiency coefficient is the highest and is equal to 10.96%. If the thickness of CMS is 6 mm, then the stress without reinforcement is 64.15 MPa, and in the case of reinforcement with transverse stiffeners equals 23.55 MPa.

The calculation of the load-bearing capacity of CMS of 6 mm thickness showed that the stresses in corrugation are 64.50 MPa and without corrugation equal to 286.00 MPa. Therefore, corrugation increases the load-bearing capacity of CMS more than four times.

Table. Technical and economic indices of design solutions

Technical solutions	Metal thickness, mm	σ_{max} MPa	σ_{el} %	C, Euro	c, Euro	E_{el} %	e_1 %
Without sheet corrugation with a thickness of 6 mm	6	286.00	0.82	223.33	–	1.00	1.82
Sheet thickness of 2 mm	2	361.60	0.65	472.00	–	1.00	1.65
Sheet thickness of 4 mm	4	126.10	1.86	943.00	–	1.00	2.86
Sheet thickness of 6 mm	6	64.15	3.66	1415.00	–	1.00	4.66
Sheet thickness of 8 mm	8	39.99	5.88	1887.00	–	1.00	6.88
Sheet thickness of 10 mm	10	28.50	8.25	2358.00	–	1.00	9.25
Reinforced with annular stiffening ribs	6	23.55	9.98	148.00	28.24	0.98	10.96

Conclusions

Based on the studies of the bearing capacity of corrugated metal structures, the following conclusions are suggested.

1. Under corrugated metal structures reinforcement with annular rods, technical and economic efficiency coefficient is the highest and equals 10.96%. If the thickness of a corrugated structure is 6 mm, then the stress without reinforcement is 64.15 MPa, and in the case of reinforcement with annular rods equals 23.55 MPa.
2. The stresses in CMS with the thickness of 6 mm and corrugation are 64.15 MPa and without corrugation equal to 286.00 MPa. Thus, corrugation increases the load-bearing capacity of the corrugated metal structure more than four times.

3. The proposed method of installing annular transverse stiffening ribs allows the restoration of the load-bearing capacity of damaged transport structures made of corrugated metal structures and increasing their service life. Compared to double corrugation, the main advantage of this method is the ability to perform structural reinforcement during construction operation without interrupting transport traffic.
4. The research has determined that the most expedient installation of the stiffeners is in the central part of the structure. The reinforcement zone of the structure is 50% wider than the width of the carriageway or railway track.

The advantage of the proposed method of increasing the load-bearing capacity of corrugated metal structures is rationally distributing the material by setting the stiffeners in the most loaded sections of corrugated metal structures.

REFERENCES

- Ahaieva, O., Karpiuk, V. M., & Posternak, O. (2019). Simulation of Design Reliability and Bearing Capacity of Normal and Oblique Sections of Span Prestressed Reinforced Concrete Structures. In *Materials Science Forum* (Vol. 968, pp. 267–280). Trans Tech Publications Ltd.
<https://doi.org/10.4028/www.scientific.net/MSF.968.267>
- Abdelkader, E., Moselhi, O., Marzouk, M., & Zayed, T. (2020). Hybrid Elman Neural Network and an Invasive Weed Optimisation Method for Bridge Defect Recognition. *Transportation Research Record*, 2675(3), 167–199.
<https://doi.org/10.1177/0361198120967943>
- Beben, D. (2009). Numerical analysis of a soil-steel bridge structure. *The Baltic Journal of Road and Bridge Engineering*, 4(1), 13–21.
<https://doi.org/10.3846/1822-427X.2009.4.13-21>
- Beben, D. (2012). Numerical study of performance of soil-steel bridge during soil backfilling. *Structural Engineering and Mechanics*, 42(4), 571–587.
- Beben, D. (2013). Field performance of corrugated steel plate road culvert under normal live-load conditions. *Journal of Performance of Constructed Facilities*, 27(6), 807–817. [https://doi.org/10.1061/\(ASCE\)CF.1943-5509.0000389](https://doi.org/10.1061/(ASCE)CF.1943-5509.0000389)
- Beben, D. (2014). Corrugated steel plate culvert response to service train loads. *Journal of Performance of Constructed Facilities*, 28(2), 376–390.
[https://doi.org/10.1061/\(ASCE\)CF.1943-5509.0000422](https://doi.org/10.1061/(ASCE)CF.1943-5509.0000422)
- Beben, D. (2017). The role of backfill quality on corrugated steel plate culvert behaviour. *The Baltic Journal of Road and Bridge Engineering*, 12(1), 1–11.
<https://doi.org/10.3846/bjrbe.2017.01>
- Contech Engineered Solutions (2019). *Structural Plate Design Guide Multi-Plate*. 7th Edition. 122 p.

- Chen, X., Zhu, Y., Cai, D., Xu, G., & Dong, T. (2020). Investigation on interface damage between cement concrete base plate and asphalt concrete waterproofing layer under temperature load in ballastless track. *Applied Sciences (Switzerland)*, 10(8), 2654. <https://doi.org/10.3390/APP10082654>
- Esmaeili, M., Zakeri, J. A., & Abdulrazagh, P. H. (2013). Minimum depth of soil cover above long-span soil-steel railway bridges. *International Journal of Advanced Structural Engineering*, 5(1), 1–17. <https://doi.org/10.1186/2008-6695-5-7>
- Flener, E. B. (2009). Response of long-span box type soil-steel composite structures during ultimate loading tests. *Journal of Bridge Engineering*, 14(6), 496–506. [https://doi.org/10.1061/\(ASCE\)BE.1943-5592.0000031](https://doi.org/10.1061/(ASCE)BE.1943-5592.0000031)
- Gerber, U., Kowaltschuk, W. W., Nabotschenko, O. S. & Sysyn, M. P. (2016). Die Tragfähigkeit von Eisenbahndurchlässen in Abhängigkeit von der Bauausführung und der Instandhaltung. *ETR – Eisenbahntechnische Rundschau*. – Euralpres, Deutschland. – Wol 5. – S. 39–44. (in German)
- Gerber, U., Sysyn, M., Zarour, J., & Nabochenko, O. (2019). Stiffness and strength of structural layers from cohesionless material. *Archives of Transport*, 49(1), 59–68. <https://doi.org/10.5604/01.3001.0013.2776>
- He, C., Zhou, S., Di, H., & Zhang, X. (2021). Effect of longitudinal joint on train-induced vibrations from subway shield-driven tunnels in a homogeneous half-space. *International Journal of Transportation Science and Technology*, in Press. <https://doi.org/10.1016/j.ijtst.2021.05.001>
- Karpiuk, V. M., Syomina, Y. A., & Antonova, D. V. (2019a). Bearing capacity of common and damaged CFRP-strengthened RC beams subject to high-level low-cycle loading. In *Materials Science Forum* (Vol. 968, pp. 185–199). Trans Tech Publications Ltd. <https://doi.org/10.4028/www.scientific.net/MSF.968.185>
- Karpiuk, V. M., Syomina, Y. A., & Antonova, D. V. (2019b). Calculation models of the bearing capacity of span reinforced concrete structure support zones. In *Materials Science Forum* (Vol. 968, pp. 209–226). Trans Tech Publications Ltd. <https://doi.org/10.4028/www.scientific.net/MSF.968.209>
- Korusiewicz, L., & Kunecki, B. (2011). Behaviour of the steel box-type culvert during backfilling. *Archives of Civil and Mechanical Engineering*, 11(3), 637–650. [https://doi.org/10.1016/S1644-9665\(12\)60106-X](https://doi.org/10.1016/S1644-9665(12)60106-X)
- Kovalchuk, V. V., Kovalchuk, Y., Sysyn, M. P., Stankevych, V. Z., & Petrenko, O. V. (2018). Estimation of carrying capacity of metallic corrugated structures of the type multiplate MP 150 during interaction with backfill soil. *Eastern-European Journal of Enterprise Technologies*, 1/1(91), 18–26. <https://doi.org/10.15587/1729-4061.2018.123002>
- Kovalchuk, V. V., Luchko, J., Bondarenko, I. O., Marcul, R. V., & Parneta, B. Z. (2016). Research and analysis of the stressed-strained state of metal corrugated structures of railroad tracks. *Eastern-European Journal of Enterprise Technologies*, 6/7(84), 4–10. <https://doi.org/10.15587/1729-4061.2016.84236>
- Kovalchuk, V. V., Marcul, R. V., Pentsak, A. Y., Parneta, B. Z., Gayda, O., & Braichenko, S. (2017). Study of the stress-strain state in defective railway

- reinforced-concrete pipes restored with corrugated metal structures. *Eastern-European Journal of Enterprise Technologies*, 5/1(89), 37–44.
<https://doi.org/10.15587/1729-4061.2017.109611>
- Kovalchuk, V., Markul, R., Bal, O., Milyanych, A., Pentsak, A., Parneta, B., & Gajda, O. (2017). The study of strength of corrugated metal structures of railroad tracks. *Eastern-European Journal of Enterprise Technologies*, 2/7(86), 18–25.
<https://doi.org/10.15587/1729-4061.2017.96549>
- Kurhan, D. (2016). Determination of Load for Quasi-static Calculations of Railway Track Stress-strain State. *Acta Technica Jaurinensis*, 9(1), 83–96.
<https://doi.org/10.14513/actatechjaur.v9.n1.400>
- Kurhan, D., Kurhan, M., & Husak, M. (2020). Impact of the variable stiffness section on the conditions of track and rolling stock interaction. *IOP Conference Series: Materials Science and Engineering*, 985(1), 012005.
<https://doi.org/10.1088/1757-899X/985/1/012005>
- Liu, Y., Hoult, N. A., & Moore, I. D. (2020). Structural performance of in-service corrugated steel culvert under vehicle loading. *Journal of Bridge Engineering*, 25(3), 04019142, 1–11.
[https://doi.org/10.1061/\(ASCE\)BE.1943-5592.0001524](https://doi.org/10.1061/(ASCE)BE.1943-5592.0001524)
- Machelski, C. (2013). Shear forces in the connection of structural elements under bending. *Studia Geotechnica et Mechanica*, 35(3), 69–83.
<https://doi.org/10.2478/sgem-2013-0031>
- Machelski, C. (2015). Stiffness of railway soil-steel structures. *Studia Geotechnica et Mechanica*, 37(4), 29–36.
<https://doi.org/10.1515/sgem-2015-0042>
- Mak, A. C., Brachman, R. W., & Moore, I. D. (2009). Measured response of a deeply corrugated box culvert to three dimensional surface loads. In *Transportation Research Board Annual Conference, Washington DC, Paper* (pp. 09-3016). 14 p.
- Maleska, T., & Beben, D. (2019). Numerical analysis of a soil-steel bridge during backfilling using various shell models. *Engineering Structures*, 196, 109358, 1–12. <https://doi.org/10.1016/j.engstruct.2019.109358>
- Nabochenko, O. S., Sysyn, M. P., Kovalchuk, V. V., Kovalchuk, Y., Pentsak, A. Y., & Braichenko, S. (2019). Studying the railroad track geometry deterioration as a result of an uneven subsidence of the ballast layer. *Eastern-European Journal of Enterprise Technologies*, 1/7(97), 50–59.
<https://doi.org/10.15587/1729-4061.2019.154864>
- Orosz, A., & Zwierczyk, P. T. (2020). Analysis of the stress state of a railway sleeper using coupled fem-dem simulation. *Proceedings – European Council for Modelling and Simulation, ECMS*, 34(1), 261–265.
- Orton, S. L., Loehr, J. E., Boeckmann, A., & Havens, G. (2015). Live-load effect in reinforced concrete box culverts under soil fill. *Journal of Bridge Engineering*, 20(11), 04015003. [https://doi.org/10.1061/\(ASCE\)BE.1943-5592.0000745](https://doi.org/10.1061/(ASCE)BE.1943-5592.0000745)
- Pettersson, L., Flener, E. B., & Sundquist, H. (2015). Design of soil-steel composite bridges. *Structural Engineering International*, 25(2), 159–172.
<https://doi.org/10.2749/101686614X14043795570499>
- Pettersson, L., Wadi, A., & Williams, K. (2017). Structural design of flexible culverts development trends. *Archiwum Instytutu Inżynierii Lądowej/ Politechnika Poznańska* 23, 237–250.

<https://doi.org/10.21008/j.1897-4007.2017.23.22>

Sanaeiha, A., Rahimian, M., & Marefat, M. S. (2017). Field test of a large-span soil-steel bridge stiffened by concrete rings during backfilling. *Journal of Bridge Engineering*, 22(10), 06017002.

[https://doi.org/10.1061/\(ASCE\)BE.1943-5592.0001102](https://doi.org/10.1061/(ASCE)BE.1943-5592.0001102)

Sheldon, T., Sezen, H., & Moore, I. D. (2015). Joint response of existing pipe culverts under surface live loads. *Journal of Performance of Constructed Facilities*, 29(1), 04014037.

[https://doi.org/10.1061/\(ASCE\)CF.1943-5509.0000494](https://doi.org/10.1061/(ASCE)CF.1943-5509.0000494)

Shvets, A., Bolotov, O., Percevoj, A., Ghlukhov, V., Bolotov, O., & Saparova, L. (2020). research of dynamic indicators and influence of different types of rolling stock on railway track. *IOP Conf. Series: Materials Science and Engineering*, 985, 012010.